

Design Technology Co-Optimization for Neuromorphic Computing

Ankita Paul, Shihao Song and Anup Das

Electrical and
Computer Engineering
Drexel University
Philadelphia, PA 19104

Email: {ankita.paul,shihao.song,anup.das}@drexel.edu

Abstract—We present a design-technology tradeoff analysis in implementing machine-learning inference on the processing cores of a Non-Volatile Memory (NVM)-based many-core neuromorphic hardware. Through detailed circuit-level simulations for scaled process technology nodes, we show the negative impact of design scaling on read endurance of NVMs, which directly impacts their inference lifetime. At a finer granularity, the inference lifetime of a core depends on 1) the resistance state of synaptic weights programmed on the core (design) and 2) the voltage variation inside the core that is introduced by the parasitic components on current paths (technology). We show that such design and technology characteristics can be incorporated in a design flow to significantly improve the inference lifetime.

I. INTRODUCTION

Neuromorphic systems are integrated circuits designed to mimic the computations in a mammalian brain [1]. They enable energy-efficient execution of Spiking Neural Networks (SNN) [2] and therefore, these systems are suitable for implementing machine learning inference tasks for embedded Systems and Edge devices in Internet-of-Things (IoT). A neuromorphic system consists of processing cores that implement neurons and synapses. Multiple such cores are interconnected together using Segmented Bus [3] or Network-on-Chip (NoC) [4] to design a many-core neuromorphic hardware [5]. Table I illustrates the neuron and synapse capacity of recent neuromorphic hardware cores.

TABLE I
CAPACITY OF RECENT NEUROMORPHIC SYSTEMS.

	ODIN	μ Brain	DYNAPs	BrainScaleS	SpiNNaker	Neurogrid	Loihi	TrueNorth
	[6]	[7]	[8]	[9]	[10]	[11]	[12]	[13]
# Neurons/core	256	336	256	512	36K	65K	130K	1M
# Synapses/core	64K	38K	16K	128K	2.8M	8M	130M	256M
# Cores/chip	1	1	1	1	144	128	128	4096
# Chips/board	1	1	4	352	56	16	768	4096
# Neurons	256	336	1K	4M	2.5B	1M	100M	4B
# Synapses	256	336	65K	1B	200B	16B	100B	1T

A neuromorphic core can be implemented using an analog crossbar where bitlines and wordlines are organized in a grid with memory cells connected at their crosspoints to store the synaptic weights [14]–[17]. Neuron circuits are implemented

along bitlines and wordlines (see Figure 2). Recently, Non-Volatile Memory (NVM) technologies such as phase-change memory (PCM) and oxide-based resistive switching random access memory (OxRRAM) are used to implement the memory cells in a neuromorphic core due to their low power consumption, CMOS-compatible scaling, and multilevel analog operations [18].¹ In an NVM-based neuromorphic inference hardware, the resistance state corresponding to the synaptic weights of an SNN are programmed on the NVM cells.

Unfortunately, NVMs suffer from reliability issues such as circuit aging, limited endurance, and read disturbance [26]–[29]. Many of these issues have been addressed recently in the context of neuromorphic computing [30]–[37]. In this work, we focus on the read disturbance issues of OxRRAM technology, where an OxRRAM cell’s resistance state may change after performing a certain number of read operations [38]–[40]. Therefore, when an OxRRAM-based neuromorphic hardware is used to implement an inference task, the trained synaptic weights programmed on the hardware may change after performing a few inference operations. To ensure expected results from an inference task, the trained weights need to be reprogrammed on to the hardware periodically. Reprogramming of synaptic weights to a neuromorphic hardware involves offlining the hardware and transferring the weights from the host to the hardware via a bandwidth-limited interconnect. This can significantly increase the overhead, and lower the availability and reliability of neuromorphic computing.

In this work, we present a design-technology tradeoff analysis in implementing machine learning inference on many-core neuromorphic hardware. Through circuit-level simulations we show the negative impact of design scaling on read endurance of NVMs, which directly impacts their inference lifetime. We show that the inference lifetime of a crossbar depends on 1) the resistance state of synaptic weights programmed on the NVMs and 2) the voltage variation inside the crossbar that is introduced by the parasitic components on current paths. Such design and technology characteristics can be incorporated in a design flow to significantly improve the inference lifetime.

¹NVMs are also used in classical von Neumann computing to mitigate the performance and energy bottleneck of DRAM [19]–[25].

II. BACKGROUND

We briefly introduce Spiking Neural Network (SNN) and their implementation in hardware.

Spiking Neural Networks (SNNs) are the third generation of neural networks designed using spiking neurons and bio-inspired learning algorithms [2]. In an SNN, spikes injected from pre-synaptic neurons raise the membrane voltage of a post-synaptic neuron (middle sub-figure of Figure 1). When the membrane voltage crosses a threshold (V_{th}), the post-synaptic neuron emits spikes that propagate to other neurons (right sub-figure of Figure 1). SNNs implement some variants of Integrate and Fire (I&F) neurons with a spike duration ranging from 1 μ s to several ms [41]–[43] (left sub-figure of Figure 1).

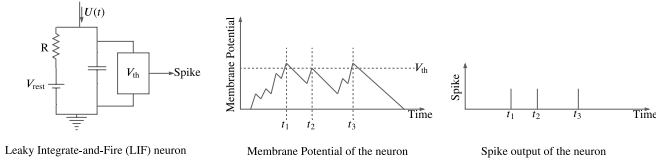


Fig. 1. A leaky integrate-and-fire (LIF) neuron. The membrane potential over time of the neuron (middle). The spike output of the neuron representing its firing time (right).

SNNs can implement many machine learning approaches [44]–[51]. In a supervised machine learning, an SNN is pre-trained with representative data. Machine-learning inference refers to feeding live data points to this trained SNN to generate the corresponding output. The quality of machine learning inference can be expressed in terms of accuracy [48], Mean Square Error (MSE) [44], Peak Signal-to-Noise Ratio (PSNR) [52], and Structural Similarity Index Measure (SSIM) [53]. For SNNs, these quality metrics are defined in terms of the inter-spike interval (ISI) [54]–[57]. If $\{t_1, t_2, \dots, t_K\}$ denote a neuron’s firing times in the time interval $[0, T]$, the average ISI of this spike train is

$$\mathcal{I} = \sum_{i=2}^K (t_i - t_{i-1}) / (K - 1). \quad (1)$$

A neuromorphic hardware platform is implemented as a tiled architecture, where tiles are interconnected via a time-multiplexed shared interconnect. Each tile consists of a neuromorphic processing core, which can implement neurons and synapses of a machine learning model. A common design practice is to use an analog crossbar to implement a core.

In a crossbar, pre-synaptic neuron circuits are placed on horizontal wires called wordlines, while post-synaptic neuron circuits are placed on vertical wires called bitlines. Memory cells are placed at the crosspoint of each wordline and bitline, and they implement the synaptic weights of an SNN. The left subfigure of Figure 2 illustrates an $N \times N$ crossbar. The right subfigure illustrates the parasitic RC components on the current path from a pre-synaptic neuron to a post-synaptic neuron accessing the memory cell (i, j) located at the crosspoint of i^{th} wordline and j^{th} bitline.

Overall, a neuromorphic hardware enables distributed and pipelined processing of SNN operations. Additionally, each

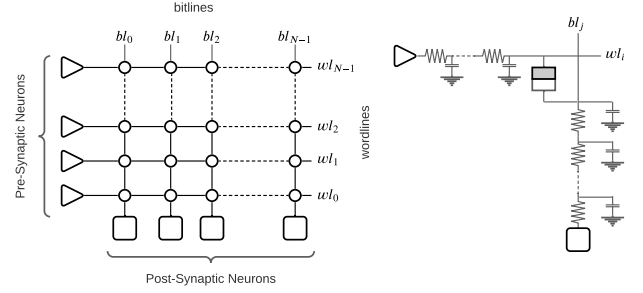


Fig. 2. An $N \times N$ crossbar showing the parasitic components within.

crossbar in the hardware can implement a maximum of N pre-synaptic neurons per post-synaptic neuron. Therefore, system-software frameworks such as NEUTRAMS [58], NeuroXplorer [59], Corelet [60], PACMAN [61], and LAVA [62] consist of 1) a compiler, which partitions an SNN model into clusters such that the neurons and synapses of each cluster can be mapped to a crossbar of the hardware, and 2) a run-time manager, which maps the clusters of an SNN to the cores of a many-core hardware. To this end, several mapping strategies have been proposed, including optimizing for energy [63]–[66], throughput [67]–[70], resource utilization [56], [58], [62], [71], [72], circuit aging [30]–[34], inference lifetime [39], and write endurance [35]–[37]. These mapping techniques all use some variant of the SNN-partitioning approach proposed in SpiNeMap [64].

Recently, dataflow models have been used to analyze performance of SNNs implemented on neuromorphic hardware, especially using Synchronous Dataflow Graphs (SDFGs) [73].² There are two strategies proposed in literature – the SDF-SNN [67] and its extended versions [68], [79], [80], which uses dataflow graphs to model an SNN, performing partitioning and mapping explorations with neurons and synapses directly, and the DFSynthesizer [69] and its extended version [70], which uses dataflow graphs to only model the clustered SNN, allowing mapping and scheduling of the clusters (a collection of neurons and synapses) to the PEs of a neuromorphic hardware.

Emerging non-volatile memory (NVM) technologies such as phase-change memory (PCM), oxide-based memory (OxRAM), spin-based magnetic memory (STT-MRAM), and Flash have recently been used for synaptic storage in crossbars. NVMs are non-volatile, have high CMOS compatibility, and can achieve high integration density. Each NVM device can implement both a single-bit and multi-bit synapse. Because of these properties, an NVM-based neuromorphic hardware typically consumes energy that is magnitudes lower than using SRAMs [81]–[83]. However, NVMs also introduce reliability issues [26]. Table II summarizes them for different NVMs.

We discuss one specific issue – limited read endurance for OxRRAM-based neuromorphic hardware.

III. INTRODUCTION TO OXIDE-BASED RESISTIVE RAM

The resistance switching random access memory (OxRRAM) technology presents an attractive option for implementing the

²SDFGs are commonly used to model streaming applications that are implemented on a multi-core system and their performance analysis [74]–[78].

TABLE II
RELIABILITY ISSUES IN NVMS.

Reliability Issues	NVMS
High-voltage related circuit aging	PCM, Flash
High-current related circuit aging	OxRRAM, STT-MRAM
Limited read endurance	All
Limited write endurance	All

synaptic cells of a crossbar due to its demonstrated potential for low-power multi-level operation and high integration density [18]. An OxRRAM cell is composed of an insulating film sandwiched between conducting electrodes forming a metal-insulator-metal (MIM) structure (see Figure 3). Recently, filament-based metal-oxide OxRRAM implemented with transition-metal-oxides such as HfO_2 , ZrO_2 , and TiO_2 has received considerable attention due to their low-power and CMOS-compatible scaling.

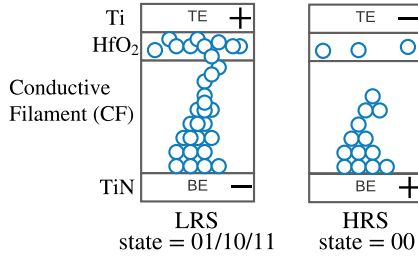


Fig. 3. Operation of an OxRRAM cell with the HfO_2 layer sandwiched between the metals Ti (top electrode) and TiN (bottom electrode). The left subfigure shows the formation of LRS states with the formation of conducting filament (CF). This represents logic states 01, 10, and 11. The right subfigure shows the depletion of CF on application of a negative voltage on the TE. This represents the HRS state or logic 00.

Synaptic weights are represented as conductance of the insulating layer within each OxRRAM cell. To program an OxRRAM cell, elevated voltages are applied at the top and bottom electrodes, which re-arranges the atomic structure of the insulating layer. Figure 3 shows the High-Resistance State (HRS) and the Low-Resistance State (LRS) of an OxRRAM cell. An OxRRAM cell can also be programmed into intermediate low-resistance states, allowing its multilevel operations.

In OxRRAM technology, the transition from HRS state is governed by a sudden decrease of the vertical filament gap on application of stress voltage during spike propagation [38]. This is illustrated in the left subfigure of Figure 4 where the vertical filament gap is shown to reduce by an amount h . This may result in a conducting filament between the two metal layers causing the resistive state to change from HRS to LRS. The rate of change of the filament gap of the OxRRAM cell at the (i, j) th location in the crossbar is

$$\frac{dg_{i,j}}{dt} = -\partial_0 \cdot e^{-\frac{E_a}{kT}} \sinh\left(\frac{\gamma_{i,j} \cdot a_0}{L} \cdot \frac{qV_{i,j}}{kT}\right), \text{ where } \gamma_{i,j} = \gamma_0 - \beta \cdot \frac{g_{i,j}^3}{g_0^3} \quad (2)$$

In the above equation, t defines the state transition time, g_0 is the initial filament gap of the OxRRAM cell, $V_{i,j}$ is the voltage applied to the cell, $\gamma_{i,j}$ is the local field enhancement factor

and is related to the gap $g_{i,j}$, a_0 is the atomic hopping distance, and γ_0 is a fitting constant.

The transition from one of the LRS states is governed by the lateral filament growth [38]. This is illustrated in the right subfigure of Figure 4. The time for state transition in the (i, j) th RRAM cell is given by

$$t_{i,j}(LRS) = 10^{-14.7 \cdot V_{i,j} + 6.7} \text{sec} \quad (3)$$

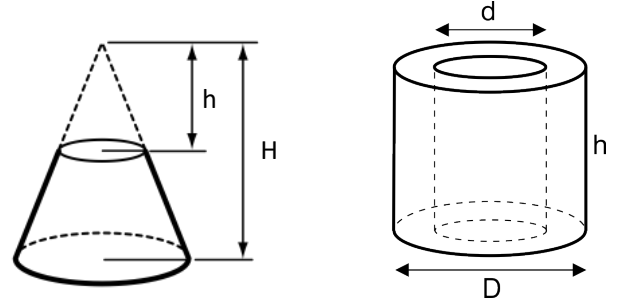


Fig. 4. Read disturbances due to structural alteration in an OxRRAM cell. The left subfigure shows a reduction of the conductive filament gap on application of a stress voltage. Such changes leads to a reduction in the resistance, i.e., a read disturbance of HRS state in the cell. The right subfigure shows the lateral growth of the conductive filament due to application of a stress voltage. This illustrates read disturbance of LRS state in the cell.

If the state transition time of an OxRRAM cell is 1000 ms, then a single quasi-static read operating using 1000 ms read pulse or 1000 read accesses using with 1-ms spike pulses can lead to an abrupt change in the state of the cell. Therefore, the endurance of the cell is 1000. If the cell propagates n spikes during inference of each image, then the inference lifetime is defined as $1000/n$. Formally,

$$\text{inference lifetime} = \frac{\text{read endurance}}{\text{spikes per image}} \quad (4)$$

IV. DESIGN-TECHNOLOGY TRADEOFF ANALYSIS

The computer memory industry has thus far been primarily driven by the cost-per-bit metric, which provides the maximum capacity for a given manufacturing cost. As shown in recent works [19]–[24], [84], manufacturing cost can be estimated from the area overhead. To estimate the cost-per-bit of a neuromorphic core, we investigate the internal architecture of a crossbar and find that a neuron circuit can be designed using 20 transistors and a capacitor [85], while an NVM cell is a 1T-1R arrangement with a transistor used as an access device for the cell. Within an $N \times N$ crossbar, there are N pre-synaptic neurons, N post-synaptic neurons, and N^2 synaptic cells. The total area of all the neurons and synapses of a crossbar is

$$\begin{aligned} \text{neuron area} &= 2N(20T + 1C) \\ \text{synapse area} &= N^2(1T + 1R) \end{aligned} \quad (5)$$

where T stands for transistor, C for capacitor, and R for NVM cell. The total synaptic cell capacity is N^2 , with each NVM cell implementing 2-bit per synapse. The total number of bits (i.e., synaptic capacity) in the crossbar is

$$\text{total bits} = 2N^2 \quad (6)$$

Therefore, the cost-per-bit of an $N \times N$ crossbar is

$$\text{cost-per-bit} = \frac{2N(20T + 1C) + N^2(1T + 1R)}{2N^2} \approx \frac{F^2(27 + 2N)}{N}, \quad (7)$$

where the cost-per-bit is represented in terms of the crossbar dimension N and the feature size F . Equation 7 provides a back-of-the-envelope calculation of cost-per-bit. Figure 5 plots the normalized cost-per-bit for four different process technology nodes, with the crossbar dimension ranging from 16 to 256. We observe that the cost-per-bit reduces with increase in the dimension of a crossbar, i.e., larger-sized crossbars can accommodate more bits for a given cost.

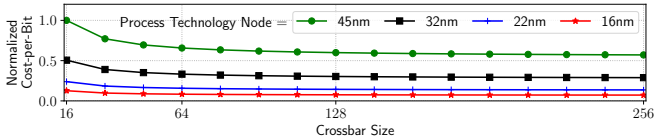
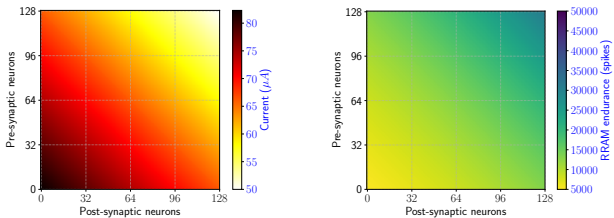


Fig. 5. Cost-per-bit analysis of a crossbar.

We now analyze the internal architecture of a crossbar. Figure 6a shows the current through the memory cells in a 128×128 crossbar. This current variation is due to the difference in the length of current paths from pre to post-synaptic neurons in the crossbar, where the length of a current path is measured in terms of the number of parasitic components on the path. These current values are obtained for a 65nm technology node and at 300K temperature corner. As can be clearly seen from the figure, current through memory cells on the top-right corner of the crossbar is lower than those at the bottom-left corner.



(a) Current map in a 128×128 crossbar. (b) RRAM endurance in a 128×128 crossbar.

Fig. 6. Current map and RRAM endurance in a 128×128 crossbar.

Figure 6b shows the endurance variation of a 128×128 crossbar at 45 nm node and at 30°C with each RRAM cell programmed to HRS state. The endurance variation is a direct result of the current variation in the crossbar.

Figure 7 shows the difference between currents on the shortest and longest paths for 32×32 , 64×64 , 128×128 , and 256×256 crossbars at 65nm process node. The input spike voltage of the pre-synaptic neurons is set to generate $50\mu\text{A}$ on the longest path. This current value corresponds to the current needed to read the resistance state of an OxRRAM cell.

We observe that the current injected into the post-synaptic neuron on the longest path is lower than the current on the shortest path by 13.3% for 32×32 , 25.1% for 64×64 , 39.2% for 128×128 , and 55.8% for 256×256 crossbar. This current difference is because of the higher voltage drop on the longest

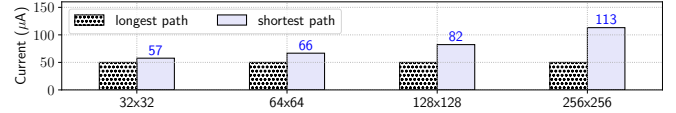


Fig. 7. Difference between current on the shortest and the longest path for different crossbar sizes.

path, which reduces the current on this path compared to the shortest path for the same amount of spike voltage applied on both these paths. The current difference increases with crossbar size because of the increase in the number of parasitic resistances on the longest current path, which results in larger voltage drops, lowering the current injected into its post-synaptic neuron. However, larger current variation causes larger endurance variation as illustrated in Figure 6b. Therefore, larger crossbar sizes leads to larger endurance variation.

System designers often make a tradeoff between cost-per-bit and endurance variation. Typically, crossbar sizes of 128×128 and 256×256 gives the best tradeoff.

V. DESIGN FLOW INCORPORATING DESIGN-TECHNOLOGY TRADEOFF

An optimized design flow is one, which takes into account the design and technology characteristics to place neurons and synapses to a crossbar such that those synapses that propagate more spikes are mapped to NVMs with higher read endurance. This is to increase the inference lifetime.

In our prior work [39], we show that such a design flow can significantly improve the inference lifetime. Figure 8 reports the inference lifetime for 10 applications for the proposed design flow normalized to SpiNeMap. We observe that through intelligent synapse mapping, the inference lifetime obtained using the proposed approach is on average 3.4x higher.

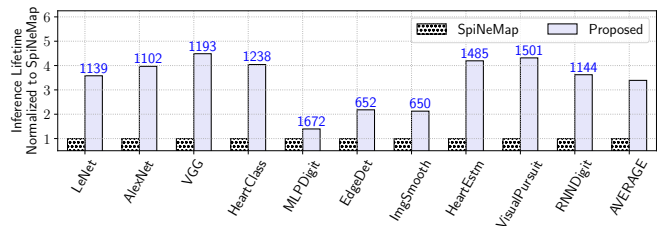


Fig. 8. Inference lifetime normalized to SpiNeMap.

VI. CONCLUSION

A design-technology tradeoff analysis is performed to investigate inference lifetime of neuromorphic hardware that adopts NVM as synaptic storage. An essential observation of the analysis is that the read endurance of an NVM cell depends on its programmed synaptic weight (design) and the voltage exposed to the cell (technology). Our analysis also reveals that voltages exposed to NVM cells inside a crossbar vary due to the parasitic components on current paths, which leads to asymmetric read endurance across NVM cells in a crossbar.

From detailed circuit-level simulations, we show design scaling on read endurance of NVMs negatively impacts the inference lifetime of neuromorphic hardware. In addition, the design flow that considers asymmetry in read endurance can significantly improve the inference lifetime of neuromorphic hardware.

ACKNOWLEDGMENT

This work is supported by the United States National Science Foundation Faculty Early Career Development Award CCF-1942697 (CAREER: Facilitating Dependable Neuromorphic Computing: Vision, Architecture, and Impact on Programmability) and the United States Department of Energy CAREER Award DE-SC0022014 (Architecting the Hardware-Software Interface for Neuromorphic Computers).

REFERENCES

- [1] C. Mead, "Neuromorphic electronic systems," *Proc. of the IEEE*, 1990.
- [2] W. Maass, "Networks of spiking neurons: The third generation of neural network models," *Neural Networks*, 1997.
- [3] A. Balaji *et al.*, "Exploration of segmented bus as scalable global interconnect for neuromorphic computing," in *GLSVLSI*, 2019.
- [4] X. Liu *et al.*, "Neu-NoC: A high-efficient interconnection network for accelerated neuromorphic systems," in *ASP-DAC*, 2018.
- [5] F. Catthoor *et al.*, "Very large-scale neuromorphic systems for biological signal processing," in *CMOS Circuits for Biological Sensing and Processing*, 2018.
- [6] C. Frenkel *et al.*, "A 0.086-mm² 12.7-pj/sop 64k-synapse 256-neuron online-learning digital spiking neuromorphic processor in 28-nm CMOS," *TBCAS*, 2018.
- [7] J. Stuijt *et al.*, "μBrain: An event-driven and fully synthesizable architecture for spiking neural networks," *Frontiers in Neuroscience*, 2021.
- [8] S. Moradi *et al.*, "A scalable multicore architecture with heterogeneous memory structures for dynamic neuromorphic asynchronous processors (DYNAPs)," *TBCAS*, 2017.
- [9] J. Schemmel *et al.*, "Live demonstration: A scaled-down version of the brainscales wafer-scale neuromorphic system," in *ISCAS*, 2012.
- [10] S. Furber *et al.*, "The SpiNNaker project," *Proc. of the IEEE*, 2014.
- [11] B. Benjamin *et al.*, "Neurogrid: A mixed-analog-digital multichip system for large-scale neural simulations," *Proceedings of the IEEE*, 2014.
- [12] M. Davies *et al.*, "Loihi: A neuromorphic manycore processor with on-chip learning," *IEEE Micro*, 2018.
- [13] M. V. Debole *et al.*, "TrueNorth: Accelerating from zero to 64 million neurons in 10 years," *Computer*, 2019.
- [14] C. Liu *et al.*, "A spiking neuromorphic design with resistive crossbar," in *DAC*, 2015.
- [15] M. Hu *et al.*, "Memristor crossbar-based neuromorphic computing system: A case study," *TNNLS*, 2014.
- [16] M. Hu *et al.*, "Dot-product engine for neuromorphic computing: Programming 1T1M crossbar to accelerate matrix-vector multiplication," in *DAC*, 2016.
- [17] A. Ankit *et al.*, "TraNNsformer: Neural network transformation for memristive crossbar based neuromorphic system design," in *ICCAD*, 2017.
- [18] A. Mallik *et al.*, "Design-technology co-optimization for OxRRAM-based synaptic processing unit," in *VLSIT*, 2017.
- [19] S. Song *et al.*, "Enabling and exploiting partition-level parallelism (PALP) in phase change memories," *TECS*, 2019.
- [20] O. Mutlu, "Memory scaling: A systems architecture perspective," in *IMW*, 2013.
- [21] S. Song *et al.*, "Improving phase change memory performance with data content aware access," in *ISMM*, 2020.
- [22] O. Mutlu *et al.*, "Research problems and opportunities in memory systems," *SUFI*, 2015.
- [23] S. Song *et al.*, "Exploiting inter- and intra-memory asymmetries for data mapping in hybrid tiered-memories," in *ISMM*, 2020.
- [24] S. Song *et al.*, "Aging-aware request scheduling for non-volatile main memory," in *ASP-DAC*, 2021.
- [25] S. Song *et al.*, "Design methodologies for reliable and energy-efficient PCM systems," in *IGSC Workshops*, 2020.
- [26] R. M. Shelby *et al.*, "Non-volatile memory as hardware synapse in neuromorphic computing: A first look at reliability issues," in *IRPS*, 2015.
- [27] L. Larcher *et al.*, "High-κ related reliability issues in advanced non-volatile memories," *Microelectronics Reliability*, 2010.
- [28] C.-Y. Lu *et al.*, "Non-volatile memory technology-today and tomorrow," in *IPFA*, 2006.
- [29] P. Noé *et al.*, "Phase-change materials for non-volatile memory devices: from technological challenges to materials science issues," *Semiconductor Science and Technology*, 2017.
- [30] S. Song *et al.*, "A case for lifetime reliability-aware neuromorphic computing," in *MWSCAS*, 2020.
- [31] A. Balaji *et al.*, "A framework to explore workload-specific performance and lifetime trade-offs in neuromorphic computing," *CAL*, 2019.
- [32] S. Song *et al.*, "Improving dependability of neuromorphic computing with non-volatile memory," in *EDCC*, 2020.
- [33] S. Kundu *et al.*, "Special session: Reliability analysis for ML/AI hardware," in *VTS*, 2021.
- [34] S. Song *et al.*, "Dynamic reliability management in neuromorphic computing," *JETC*, 2021.
- [35] T. Titirsha *et al.*, "Reliability-performance trade-offs in neuromorphic computing," in *IGSC Workshops*, 2020.
- [36] T. Titirsha *et al.*, "Thermal-aware compilation of spiking neural networks to neuromorphic hardware," in *LCPC*, 2020.
- [37] T. Titirsha *et al.*, "Endurance-aware mapping of spiking neural networks to neuromorphic hardware," *TPDS*, 2021.
- [38] W. Shim *et al.*, "Impact of read disturb on multilevel RRAM based inference engine: Experiments and model prediction," in *IRPS*, 2020.
- [39] S. Song *et al.*, "Improving inference lifetime of neuromorphic systems via intelligent synapse mapping," in *ASAP*, 2021.
- [40] K.-T. Chen *et al.*, "Non-volatile ferroelectric FETs using 5-nm Hf 0.5 Zr 0.5 O 2 with high data retention and read endurance for 1T memory applications," *EDL*, 2019.
- [41] S. Fusi *et al.*, "Collective behavior of networks with linear (VLSI) integrate-and-fire neurons," *Neural Computation*, 1999.
- [42] S. Zhang *et al.*, "A pulse-width modulation neuron with continuous activation for processing-in-memory engines," in *DATE*. IEEE, 2020.
- [43] A. J. Leigh *et al.*, "An efficient spiking neuron hardware system based on the hardware-oriented modified Izhikevich neuron (HOMIN) model," *TCAS II: Express Briefs*, 2020.
- [44] A. Das *et al.*, "Unsupervised heart-rate estimation in wearables with Liquid states and a probabilistic readout," *Neural Networks*, 2018.
- [45] E. J. Moyer *et al.*, "Machine learning applications to DNA subsequence and restriction site analysis," in *SPMB*, 2020.
- [46] J. P. Dominguez-Morales *et al.*, "Deep spiking neural network model for time-variant signals classification: a real-time speech recognition approach," in *IJCNN*, 2018.
- [47] A. Das *et al.*, "Heartbeat classification in wearables using multi-layer perceptron and time-frequency joint distribution of ECG," in *CHASE*, 2018.
- [48] A. Balaji *et al.*, "Power-accuracy trade-offs for heartbeat classification on neural networks hardware," *JOLPE*, 2018.
- [49] Q. Yu *et al.*, "A spiking neural network system for robust sequence recognition," *TNNLS*, 2015.
- [50] S. Schliebs *et al.*, "Evolving spiking neural network—a survey," *Evolving Systems*, 2013.
- [51] M. Dong *et al.*, "Unsupervised speech recognition through spike-timing-dependent plasticity in a convolutional spiking neural network," *PLoS one*, 2018.
- [52] T. Chou *et al.*, "CARLsim 4: An open source library for large scale, biologically detailed spiking neural network simulation using heterogeneous clusters," in *IJCNN*, 2018.
- [53] A. Hore *et al.*, "Image quality metrics: PSNR vs. SSIM," in *ICPR*, 2010.
- [54] P. A. Cariani, "Temporal coding of sensory information in the brain," *Acoustical Science and Technology*, 2001.
- [55] H. Fang *et al.*, "Encoding, model, and architecture: systematic optimization for spiking neural network in FPGAs," in *ICCAD*, 2020.
- [56] A. Balaji *et al.*, "PyCARL: A PyNN interface for hardware-software co-simulation of spiking neural network," in *IJCNN*, 2020.
- [57] M. Kiselev, "Rate coding vs. temporal coding-is optimum between?" in *IJCNN*, 2016.
- [58] Y. Ji *et al.*, "NEUTRAMS: Neural network transformation and co-design under neuromorphic hardware constraints," in *MICRO*, 2016.
- [59] A. Balaji *et al.*, "NeuroXplorer 1.0: An extensible framework for architectural exploration with spiking neural networks," in *ICONS*, 2021.

- [60] A. Amir *et al.*, "Cognitive computing programming paradigm: a corelet language for composing networks of neurosynaptic cores," in *IJCNN*, 2013.
- [61] F. Galluppi *et al.*, "A hierarchical configuration system for a massively parallel neural hardware platform," in *CF*, 2012.
- [62] C.-K. Lin *et al.*, "Mapping spiking neural networks onto a manycore neuromorphic architecture," in *PLDI*, 2018.
- [63] A. Das *et al.*, "Mapping of local and global synapses on spiking neuromorphic hardware," in *DATE*, 2018.
- [64] A. Balaji *et al.*, "Mapping spiking neural networks to neuromorphic hardware," *TVLSI*, 2020.
- [65] T. Titirsha *et al.*, "On the role of system software in energy management of neuromorphic computing," in *CF*, 2021.
- [66] A. Balaji *et al.*, "Run-time mapping of spiking neural networks to neuromorphic hardware," *JSPS*, 2020.
- [67] A. Das *et al.*, "Dataflow-based mapping of spiking neural networks on neuromorphic hardware," in *GLSVLSI*, 2018.
- [68] A. Balaji *et al.*, "A framework for the analysis of throughput-constraints of SNNs on neuromorphic hardware," in *ISVLSI*, 2019.
- [69] S. Song *et al.*, "Compiling spiking neural networks to neuromorphic hardware," in *LCTES*, 2020.
- [70] S. Song *et al.*, "DFSynthesizer: Dataflow-based synthesis of spiking neural networks to neuromorphic hardware," *TECS*, 2021.
- [71] A. Balaji *et al.*, "Enabling resource-aware mapping of spiking neural networks via spatial decomposition," *ESL*, 2020.
- [72] A. Balaji *et al.*, "Compiling spiking neural networks to mitigate neuromorphic hardware constraints," in *IGSC Workshops*, 2020.
- [73] E. Lee *et al.*, "Synchronous data flow," *Proceedings of the IEEE*, 1987.
- [74] S. Sriram *et al.*, *Embedded Multiprocessors; Scheduling and Synchronization*, 2000.
- [75] L. Jiashu *et al.*, "A design flow for partially reconfigurable heterogeneous multi-processor platforms," in *RSP*, 2012.
- [76] A. Das *et al.*, *Reliable and Energy Efficient Streaming Multiprocessor Systems*. Springer, 2018.
- [77] A. Das *et al.*, "Reliability and energy-aware mapping and scheduling of multimedia applications on multiprocessor systems," *TPDS*, 2015.
- [78] A. H. Ghamarian *et al.*, "Throughput analysis of synchronous data flow graphs," in *ACSD*, 2006.
- [79] S. Song *et al.*, "A design flow for mapping spiking neural networks to many-core neuromorphic hardware," in *ICCAD*, 2021.
- [80] S. Curzel *et al.*, "Automated generation of integrated digital and spiking neuromorphic machine learning accelerators," in *ICCAD*, 2021.
- [81] G. W. Burr *et al.*, "Neuromorphic computing using non-volatile memory," *Advances in Physics: X*, 2017.
- [82] S. Kim *et al.*, "NVM neuromorphic core with 64k-cell (256-by-256) phase change memory synaptic array with on-chip neuron circuits for continuous in-situ learning," in *IEDM*, 2015.
- [83] S. B. Eryilmaz *et al.*, "Device and system level design considerations for analog-non-volatile-memory based neuromorphic architectures," in *IEDM*, 2015.
- [84] D. Lee *et al.*, "Tiered-latency DRAM: A low latency and low cost DRAM architecture," in *HPCA*, 2013.
- [85] G. Indiveri, "A low-power adaptive integrate-and-fire neuron circuit," in *ISCAS*, 2003.